An Improved Third-order CWENO-Z Scheme at critical points

IOP Conf. Series: Materials Science and Engineering **569** (2019) 032031 doi:10.1088/1757-899X/569/3/032031

An Improved Third-order CWENO-Z Scheme at critical points

Shujiang Tang[1,2], Mingjun Li[1*], Shuang Han[1]

[1]School of mathematics and computational science, Xiangtan University, Xiangtan, Hunan, 411105, China

[2]Hunan Key Laboratory for Computation and Simulation in Science and Engineering , Xiangtan, Hunan, 411105, China

[*]Corresponding author's e-mail: limingjun@xtu.edu.cn

Abstract. In this paper, by modifying the smoothness factor of the third-order CWENO scheme, we present the two-parameter CWENO-NZ3 scheme to improve accuracy at critical points. We selected some classical examples for numerical simulation, such as one-dimensional Sod shock tube, Shock-entropy wave interaction, Riemann problem with strong discontinuity and Rayleigh-Taylor instability problem. Numerically comparing with the classical third-order CWENO schemes, it is found that the improved schemes not only improve accuracy and resolution at the extreme points, but also reduce dissipation.

1. Introduction

Based on ENO scheme, through reconstructing weights of stencil of WENO scheme, it solves the problem of wasting a lot of computation in the smooth region of the solution of ENO [1]. Many scholars have also done a lot of research on WENO scheme, and have created various types of WENO scheme [2-4]. In 2005, Henrick et al. [5] found that the convergence condition of five-order WENO scheme is not sufficient, and the accuracy of continuous solutions at extreme points will reduce the order. In view of this defect, they proposed the concept of mapping weight and constructed a new weighted scheme WENO–M scheme. In 2008, Borges et al. [6] constructed a high resolution WENO–Z scheme with lower dissipation by constructing global high order smooth factors through linear combination of low order candidate stencil smooth factors on the basis of classical WENO scheme. In 2013, Yamaleey et al. [7] theoretically deduced a class of third-order energy-stable WENO scheme (ESWENO) by improving the global smooth factor in the third-order WENO scheme. Wu et al. [8-10] proposed an improved third-order WENO scheme (WENO–N3, WENO–NP3 and WENO–NN3) by introducing the global stencil smoothing factor through theoretical derivation, aiming at the linearity of the traditional third-order WENO–Z scheme that reduces the order at the extreme point. In 2016, Acker et al. [11] improved WENO–Z scheme by locally increasing the influence of non-smooth regions, and deduced the third-order WENO–Z3+ and fifth-order WENO –Z5+ schemes with high resolution.

The above WENO schemes are essentially upwind TVD schemes. With the development of the central schemes, many scholars have combined WENO scheme and the central scheme to construct many improved central schemes with high accuracy and high resolution. Levy et al. [12] firstly combined the full discrete central scheme with the reconstruction idea of WENO scheme, and constructed a new class of WENO scheme, the central WENO scheme (CWENO). Since the CWENO

scheme not only has the advantages of the central scheme not limited to specific problems, but also has the physical properties of upwind scheme. Since the concept of the CWENO scheme was put forward, it has been widely concerned by scholars. In 2002, Qiu and Shu [13] constructed a class of the fifth-order CWENO schemes by using Lax-Wendroff time discretization, and then they further improved accuracy of CWENO scheme to ninth order. In 2018, take advantage of the low dissipation and high resolution of WENO-Z scheme, Cravero et al. [14] firstly introduced weight coefficient of WENO-Z scheme into CWENO scheme, and established a new CWENO-Z scheme with higher resolution.

On the basis of the above research, we reconstruct the two-parameter CWENO-NZ3 scheme by modifying the smoothness factor.

2. Governing equation

The one-dimensional hyperbolic conservation law equation can be represented as

$$u_t + f(u)_x = 0, \tag{1}$$

Suppose the solution region [a,b] is divided as

$$a = x_{1/2} < x_{3/2} < \cdots < x_{N-1/2} < x_{N+1/2} = b, \tag{2}$$

The center is $x_j = \frac{1}{2}\left(x_{j-1/2} + x_{j+1/2}\right)$ in the cell $I_j = \left[x_{j-1/2}, x_{j+1/2}\right]$, and cell sizes $\Delta x_j = x_{j+1/2} - x_{j-1/2}$. Then we define the average value $\bar{u}_j = \frac{1}{\Delta x}\int_{I_j} u\left(x, t^n\right)dx$ in the cell I_j. So that the integration of (1) over the rectangle $\left[x_j, x_{j+1}\right]\times\left[t^n, t^{n+1}\right]$ divided by Δx_j is the following semi-discrete form

$$\frac{d}{dt}\bar{u}_j + \frac{1}{\Delta x}\left(f_{j+1/2} - f_{j-1/2}\right) = 0, \tag{3}$$

where $f_{j\pm1/2}$ indicate the flux at $x_{j\pm1/2}$.

Assume the value of $u_{j\pm1/2}$ have been restructured. In order to transform (3) into a finite volume scheme, the flux should be expressed by the cell average value $\bar{u}_j$. Considering the solution of (1) must satisfy upwind characteristics, we suppose $f_{j\pm1/2} = \hat{f}\left(u^R_{j\pm1/2}, u^L_{j\pm1/2}\right)$, where $\hat{f}$ satisfies monotonicity, compatibility and local Lipschitz continuity. In this paper, we will use the following Lax-Friedrichs numerical flux

$$\hat{f}\left(u^R_{j\pm1/2}, u^L_{j\pm1/2}\right) = \frac{1}{2}\left(f^R_{j\pm1/2} + f^L_{j\pm1/2} - c_{j\pm1/2}\left(u^R_{j\pm1/2} - u^L_{j\pm1/2}\right)\right), \tag{4}$$

where, $f^R_{j\pm1/2} = f\left(u^R_{j\pm1/2}\right)$, $f^L_{j\pm1/2} = f\left(u^L_{j\pm1/2}\right)$. $u^L_{j\pm1/2}$ and $u^R_{j\pm1/2}$ are values on the left and right sides of points $x_{j\pm1/2}$, which will be reconstructed from the following third-order and fifth-order CWENO schemes. And $c_{j\pm1/2}$ indicate spectral radius of Jacobian matrix corresponding to (1) at the points $x_{j\pm1/2}$. Time evolution of the governing equation will be carried out by the classical third-order Runge-Kutta TVD scheme.

3. Third-order CWENO schemes

We reconstruct a quadratic polynomial $\widetilde{P}_j(x)$ as the convex combination of three order linear polynomials of $P^n_{j-1}(x)$, $P^n_j(x)$ and $P^n_{j+1}(x)$ in every cell $I_j = \left[x_{j-1/2}, x_{j+1/2}\right]$,

$$\widetilde{P}_j(x)=\omega_{j-1}^n P_{j-1}^n(x)+\omega_j^n P_j^n(x)+\omega_{j+1}^n P_{j+1}^n(x), \tag{5}$$

where $\omega_k^n(k=j-1,j,j+1)$ is weight coefficient, $\sum_k \omega_k^n=1$. The polynomials $P_{j-1}^n(x)$ and $P_{j+1}^n(x)$ correspond to one-sided linear reconstruction on the left and right sides, however the polynomial $P_j^n(x)$ is a parabola at central point x_j.

$$\begin{aligned}
&P_{j-1}^n(x)=\bar{u}_j+\frac{\bar{u}_j-\bar{u}_{j-1}}{\Delta x}(x-x_j),\\
&P_{j+1}^n(x)=\bar{u}_j+\frac{\bar{u}_{j+1}-\bar{u}_j}{\Delta x}(x-x_j),\ P_j^n(x)=\bar{u}_j+\frac{\bar{u}_{j+1}-\bar{u}_{j-1}}{2\Delta x}(x-x_j).
\end{aligned} \tag{6}$$

It is noted that $P_j^n(x)$ is only a parabola which satisfies the conservation of $\bar{u}_{j-1}^n$、$\bar{u}_j^n$ and $\bar{u}_{j+1}^n$ on three grids. Therefore, the polynomial can be rewritten

$$\widetilde{P}_j(x)=u_j+u'(x-x_j)+\frac{1}{2}u''(x-x_j)^2, \tag{7}$$

where u_j and derivative u_j' and u_j'' are given as follows

$$u_j=\bar{u}_j^n-\frac{\omega_j^n}{12}\left(\bar{u}_{j+1}^n-2\bar{u}_j^n+\bar{u}_{j-1}^n\right),\ u_j'=\frac{1}{\Delta x}\left(\omega_j^n\left(\bar{u}_j^n-\bar{u}_{j-1}^n\right)+\omega_j^n\frac{\bar{u}_{j+1}^n-\bar{u}_{j-1}^n}{2}+\omega_j^n\left(\bar{u}_{j+1}^n-\bar{u}_j^n\right)\right),$$

$$u_j''=2\omega_j^n\frac{\bar{u}_{j+1}^n-2\bar{u}_j^n+\bar{u}_{j-1}^n}{(\Delta x)^2}. \tag{8}$$

3.1. CWENO-JS3 scheme

The so-called CWENO-JS3 [2] are defined by

$$\omega_k^n=\frac{\alpha_k^n}{\alpha_{j-1}^n+\alpha_j^n+\alpha_{j+1}^n},\quad k=j-1,j,j+1 \tag{9}$$

where $\alpha_k^n=\frac{C_k}{(\varepsilon+IS_k^n)^q}$, $k=j-1,\ j,j+1$. Constants C_k are linear weights which are defined as $C_{j-1}=C_{j+1}=1/4$, $C_j=1/2$. The constant ε is used to ensure the denominator is not zero, $\varepsilon=10^{-6}$ and $q=2$. IS_k^n are smoothness factor,

$$IS_k^n=\sum_{l=1}^{2}\int_{x-1/2}^{x+1/2}(\Delta x)^{2l-1}\left(P_k^{(l)}(x)\right)^2dx,\quad k=j-1,\ j,\ j+1. \tag{10}$$

$P_k^{(l)}(x)$ is the l-order derivative of $P_k(x)$. Then we can calculate integrals in (10)

$$IS_{j-1}^n=\left(\bar{u}_j^n-\bar{u}_{j-1}^n\right)^2,IS_j^n=\frac{13}{3}\left(\bar{u}_{j+1}^n-2\bar{u}_j^n+\bar{u}_{j-1}^n\right)^2+\frac{1}{4}\left(\bar{u}_{j+1}^n-\bar{u}_{j-1}^n\right)^2,IS_{j+1}^n=\left(\bar{u}_{j+1}^n-\bar{u}_j^n\right)^2. \tag{11}$$

3.2. CWENO-Z3 scheme

Borges et al. [6] constructed the high resolution WENO-Z scheme as follows

$$\alpha_k^n = d_k\left[1+\left(\frac{\tau}{\beta_k+\varepsilon}\right)^q\right],\ \ k=0,1 \tag{12}$$

where, $d_0 = 1/3$, $d_1 = 2/3$, $\beta_0 = \left(\bar{u}_j^n - \bar{u}_{j-1}^n\right)^2$, $\beta_1 = \left(\bar{u}_{j+1}^n - \bar{u}_j^n\right)^2$. The global smoothness factor τ is defined as $\tau = \left|\beta_0 - \beta_1\right|$.

Similarly, the smoothness factor are proposed by ref. [14]

$$\alpha_k^n = C_k\left[1+\left(\frac{\tau}{IS_k+\varepsilon}\right)^q\right],\ \ k=j-1,j,j+1 \tag{13}$$

where $\tau = \left|IS_{j-1} - IS_{j+1}\right|$, $C_{j-1} = C_{j+1} = 1/4$, $C_j = 1/2$, they called it CWENO-Z3.

3.3. CWENO-Z3+ scheme

Acker et al. [7] constructed the WENO-Z3+ scheme as follows

$$\alpha_k^n = d_k\left[1+\left(\frac{\tau}{\beta_k+\varepsilon}\right)^q+\zeta_k\right],\ \ k=0,1 \tag{14}$$

where ζ_k is an undetermined smoothness factor, which is simply proposed $\zeta_k = \lambda\left(\frac{\beta_k+\varepsilon}{\tau+\varepsilon}\right)$ by Acker, where λ is an empirical constant whose value depends on the size of the grid. Usually $\lambda = 0$, then WENO-Z3+ degenerates into WENO-Z3.

As CWENO scheme is only weighted by global stencils of WENO scheme, we can directly introduce idea of WENO-Z3+ scheme into CWENO scheme. Then central WENO-Z3+ scheme (CWENO-Z3+) is reconstructed as follows

$$\alpha_k^n = C_k\left[1+\left(\frac{\tau}{IS_k+\varepsilon}\right)^q+\lambda\frac{IS_k+\varepsilon}{\tau+\varepsilon}\right],\ \ k=j-1,j,j+1$$
$$\tau = \left|IS_{j-1} - IS_{j+1}\right|. \tag{15}$$

We simply select $\lambda = 1$ in this paper.

3.4. The two-parameter CWENO-NZ3 scheme

Wu et al. [8] constructed the WENO-NZ3 scheme as follows

$$\alpha_k^n = d_k\left[1+\frac{\tau_{NP}}{\beta_k+\varepsilon}\right],\ \ k=0,1$$
$$\tau_{NP} = \left|\frac{\beta_0-\beta_1}{2}-\beta_2\right|^N,\ N=3/2 \tag{16}$$

where $\beta_2 = \frac{13}{12}\left(\bar{u}_{j+1}^n - 2\bar{u}_j^n + \bar{u}_{j-1}^n\right)^2 + \frac{1}{4}\left(\bar{u}_{j+1}^n - \bar{u}_{j-1}^n\right)^2$.

Then Wu et al. [9, 10] improved the WENO-NP3 scheme to construct the WENO-NN3 scheme

$$\alpha_k^n = d_k\left[1+\left(\frac{\tau_N}{(\beta_k+\varepsilon)^q}\right)\right],\ \ k=0,1$$
$$\tau_N = \left|\frac{\beta_0-\beta_1}{2}-\beta_2\right|, \tag{17}$$

here β_2 is called a global stencil smoothness factor, its value has a similar structure to the IS_j^n in CWENO, it's just the coefficients that are different.

Next, based on the above two CWENO scheme and Taylor's mean value theorem, we construct the third-order two-parameter-CWENO-NZ3 scheme as follows

$$\alpha_k^n = C_k\left[1+\left(\frac{\tau_N}{\left(IS_k^n+\varepsilon\right)^q}\right)\right],\quad k=j-1,j,j+1 \tag{18-1}$$

$$\tau_N = \left|\frac{IS_{j+1}^n + IS_{j-1}^n}{2} - IS_j^n\right|^N, \tag{18-2}$$

where $\varepsilon = 10^{-40}$, N and q are the parameters which are determined by Taylor's formula, meanwhile $q \neq 0$.

Here, we give the calculation process of the weight function in the third-order two-parameter CWENO-NZ3 scheme in detail. Calculate (11) by Taylor series expansion at the non-extreme point of continuous solution

$$\begin{aligned}
IS_{j-1}^n &= \left(u_j'\right)^2(\Delta x)^2 - u_j'u_j'''(\Delta x)^3 + \left(\frac{1}{4}\left(u_j''\right)^2 + \frac{1}{3}u_j'u_j''\right)(\Delta x)^4 - \left(\frac{1}{12}u_j'u_j^{(4)} + \frac{1}{6}u_j''u_j'''\right)(\Delta x)^5 \\
&\quad + \left(\frac{1}{60}u_j'u_j^{(5)} + \frac{1}{24}u_j''u_j^{(4)} + \frac{1}{36}\left(u_j'''\right)^2\right)(\Delta x)^6 + \mathrm{O}\left((\Delta x)^7\right), \\
IS_j^n &= \left(u_j'\right)^2(\Delta x)^2 + \left(\frac{13}{3}\left(u_j''\right)^2 + \frac{1}{3}u_j'u_j'''\right)(\Delta x)^4 + \left(\frac{1}{60}u_j'u_j^{(5)} + \frac{13}{18}u_j''u_j^{(4)} + \frac{1}{36}\left(u_j'''\right)^2\right)(\Delta x)^6 + \mathrm{O}\left((\Delta x)^7\right), \\
IS_{j+1}^n &= \left(u_j'\right)^2(\Delta x)^2 + u_j'u_j'''(\Delta x)^3 + \left(\frac{1}{4}\left(u_j''\right)^2 + \frac{1}{3}u_j'u_j''\right)(\Delta x)^4 + \left(\frac{1}{12}u_j'u_j^{(4)} + \frac{1}{6}u_j''u_j'''\right)(\Delta x)^5 \\
&\quad + \left(\frac{1}{60}u_j'u_j^{(5)} + \frac{1}{24}u_j''u_j^{(4)} + \frac{1}{36}\left(u_j'''\right)^2\right)(\Delta x)^6 + \mathrm{O}\left((\Delta x)^7\right),
\end{aligned} \tag{19}$$

u_j'、u_j''、u_j''' represent first-order, second-order and third-order spatial derivatives respectively. Substitute (19) into (18-2),

$$\left|\frac{IS_{j+1}^n + IS_{j-1}^n}{2} - IS_j^n\right| = \frac{49}{12}\left(u_j''\right)^2(\Delta x)^4 + \frac{39}{72}u_j''u_j{}^4(\Delta x)^6 + \mathrm{O}\left((\Delta x)^7\right), \tag{20}$$

Thus, at the first-order extreme point $\left(u_j' = 0,\ u_j'' \neq 0\right)$

$$\begin{aligned}
IS_{j-1}^n &= \frac{1}{4}\left(u_j''\right)^2(\Delta x)^4 - \frac{1}{6}u_j''u_j'''(\Delta x)^5 + \left(\frac{1}{24}u_j''u_j^{(4)} + \frac{1}{36}\left(u_j'''\right)^2\right)(\Delta x)^6 + \mathrm{O}\left((\Delta x)^7\right), \\
IS_j^n &= \frac{13}{3}\left(u_j''\right)^2(\Delta x)^4 + \left(\frac{13}{18}u_j''u_j^{(4)} + \frac{1}{36}\left(u_j'''\right)^2\right)(\Delta x)^6 + \mathrm{O}\left((\Delta x)^7\right), \\
IS_{j+1}^n &= \frac{1}{4}\left(u_j''\right)^2(\Delta x)^4 + \frac{1}{6}u_j''u_j'''(\Delta x)^5 + \left(\frac{1}{24}u_j''u_j^{(4)} + \frac{1}{36}\left(u_j'''\right)^2\right)(\Delta x)^6 + \mathrm{O}\left((\Delta x)^7\right),
\end{aligned} \tag{21}$$

Substitute (19), (21) into (18-1), we obtain

$$\alpha_{j-1}^n = C_{j-1}\left[1 + \frac{49^N 4^q}{12^N}\left(u_j''\right)^{2(N-q)}(\Delta x)^{4(N-q)} + \frac{2Z}{3}\frac{49^N 4^q}{12^N}\left(u_j''\right)^{2(N-q)-1}u_j'''(\Delta x)^{4(N-q)+1} + \mathrm{O}\left((\Delta x)^{4(N-q)+2}\right)\right],$$

$$\alpha_j^n = C_j\left[1+\frac{49^N 3^q}{12^N 13^q}\left(u_j''\right)^{2(N-Z)}(\Delta x)^{4(N-q)} - \frac{49^N 3^{q-1}}{12^N 13^{q-1}}\left(u_j''\right)^{2(N-q)-2}\right.$$
$$\left.\times\left(\frac{1}{36}\left(u_j'''\right)^2+\frac{13}{18}u_j''u_j^{(4)}\right)(\Delta x)^{4(N-q)+2}+\mathrm{O}\left((\Delta x)^{4(N-q)+3}\right)\right],$$
$$\alpha_{j+1}^n = C_{j+1}\left[1+\frac{49^N 4^q}{12^N}\left(u_j''\right)^{2(N-q)}(\Delta x)^{4(N-Z)} - \frac{2Z}{3}\frac{49^N 4^q}{12^N}\left(u_j''\right)^{2(N-q)-1}u_j'''(\Delta x)^{4(N-q)+1}+\mathrm{O}\left((\Delta x)^{4(N-q)+2}\right)\right], \tag{22}$$

Substitute $C_{j-1}=C_{j+1}=1/4$, $C_j=1/2$ and $\beta_2=\frac{13}{12}\left(\bar{u}_{j+1}^n-2\bar{u}_j^n+\bar{u}_{j-1}^n\right)^2+\frac{1}{4}\left(\bar{u}_{j+1}^n-\bar{u}_{j-1}^n\right)^2$ into (5), we obtain the following weight coefficients

$$\omega_{j-1}^n = \frac{1}{4}+\frac{49^N}{8\cdot 12^N}\left[4^Z-\left(\frac{3}{13}\right)^q\right]\left(u_j''\right)^{2(N-q)}(\Delta x)^{4(N-q)}+\mathrm{O}\left((\Delta x)^{4(N-q)+1}\right),$$
$$\omega_j^n = \frac{1}{2}+\frac{49^N}{4\cdot 12^N}\left[4^q-\left(\frac{3}{13}\right)^q\right]\left(u_j''\right)^{2(N-q)}(\Delta x)^{4(N-q)}+\mathrm{O}\left((\Delta x)^{4(N-q)+1}\right),$$
$$\omega_{j+1}^n = \frac{1}{4}+\frac{49^N}{8\cdot 12^N}\left[4^q-\left(\frac{3}{13}\right)^q\right]\left(u_j''\right)^{2(N-q)}(\Delta x)^{4(N-q)}+\mathrm{O}\left((\Delta x)^{4(N-q)+1}\right). \tag{23}$$

Combining the above process, we realize the following results

Theorem A For the two-parameter-CWENO-NZ3 scheme, if $N-q\geq 1/2, q\neq 0$, then the scheme has third-order accuracy.

Considering the CWENO-NZ3 scheme has two parameters, we always choose $N=q+1.$

4. Numerical results

4.1 one-dimensional problem

No special explanation required, we choose the CFL=0.5 and $\gamma=1.4$ for two one-dimensional problems in the following.

4.1.1 Sod shock tube

Initial conditions[15]

$$(\rho,u,p)=\begin{cases}(1,0,1) & 0\leq x<0.5\\ (0.125,0,0.1), & 0.5\leq x\leq 1\end{cases}$$

In this example, the tight support boundary condition is used on both sides of the left and right ends, the calculation region is [0,1]. The figures show the density of the solution using three kinds of FWENO schemes at t=0.1644, n=400 uniform grids were used. Fig. 1 shows the results of the third-order scheme using the ACM corrector method proposed by Harten et al. to suppress oscillation. It can be clearly seen from the Fig.1 that CWENO-NZ3 has the best computational performance.

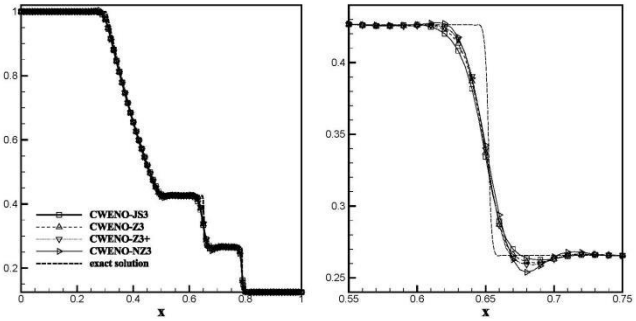

Figs. 1: Sod problem: density curve and partially enlarged detail at the final time

4.1.2 Shu-Osher problem
Initial conditions[2]

$$(\rho, u, p) = \begin{cases} (3.857143, 2.629369, 10.33333) & -5 \le x < -4 \\ (1 + 0.2sin(5x), 0, 1), & -4 \le x \le 5 \end{cases}$$

In this example, the tight support boundary condition is used on both sides of the left and right ends, the calculation region is [-6,6]. The figures show the density of the solution using three kinds of FWENO schemes at t=1.8, n=800 uniform grids were used. Fig. 2.3 shows the results of the third-order scheme using the ACM corrector method. From Fig. 2.3, it is obvious that the improved CWENO-NZ3 scheme has the best computational performance.

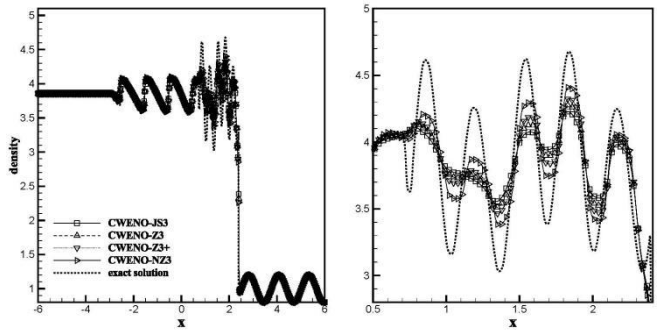

Figs. 2: Shu-Osher problem: density curve and partially enlarged detail at the final time

4.2 two-dimensional problem
In the following two-dimensional Riemann problems, the CFL number is 0.2 and the adiabatic index $\gamma = 1.4$. In the Rayleigh-Taylor instability problem, the CFL number is 0.45 and the adiabatic index $\gamma = 1.667$. For CWENO-NZ3, we always take $N = Z + 1$.

4.2.1 Riemann problem
Initial conditions[16]

$$(\rho, u, \mathrm{v}, p) = \begin{cases} (2, 0.75, 0.5, 1), & x < 0.5, y > 0.5 \\ (1, 0.75, -0.5, 1), & x > 0.5, y > 0.5 \\ (1, -0.75, 0.5, 1), & x < 0.5, y < 0.5 \\ (3, -0.75, -0.5, 1), & x > 0.5, y < 0.5 \end{cases}$$

In this example, the free interface is used in the upper and lower boundaries, the calculation region is $[0,1]\times[0,1]$. Fig. 3 shows the figures show the density of the solution using three kinds of FWENO schemes at t=0.6, nXn =800X800 uniform grids were used. It can be clearly seen from Fig. 3 that the

vortex structure of the improved CWENO-NZ3 scheme is the clearest, which shows that the scheme has the best computational performance. Compared with CWENO-JS3 and CWENO-Z3, the CWENO-NP3 scheme not only has lower dissipation, but also has higher accuracy.

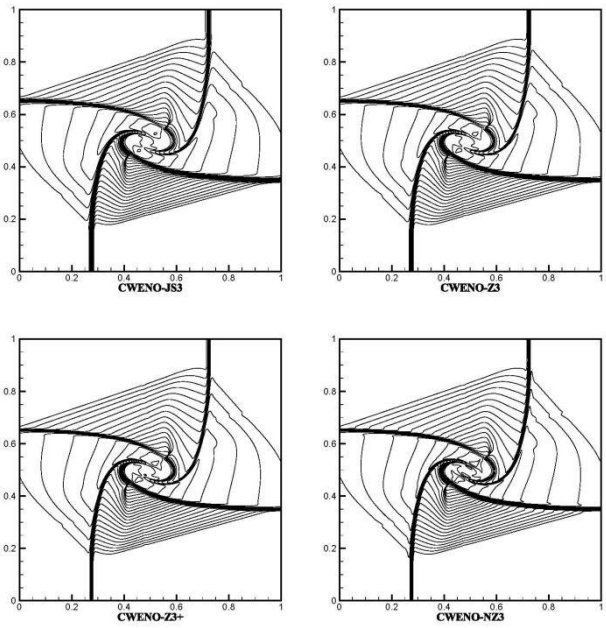

Figs. 3: Riemann problem: 40 density contours at the final time

4.2.2 Rayleigh-Taylor instability problem
Initial conditions[2]

$$(\rho,u,\mathrm{v},p)=\begin{cases}(2,0,-0.025\sqrt{\gamma p/\rho}cos(8\pi x),2\mathrm{y}+1), & 0\le y<0.5\\ (1,0,-0.025\sqrt{\gamma p/\rho}cos(8\pi x),\mathrm{y}+1.5), & 0.5\le x<1\end{cases}$$

In this example, the calculation region is $[0,0.25]\times[0,1]$, the left and right boundary conditions are reflection boundary conditions, and the top and bottom boundary conditions are respectively, $(\rho,u,\mathrm{v},p)=(1,0,0,2.5)$, $(\rho,u,\mathrm{v},p)=(2,0,0,1)$. Fig. 4 shows the calculation results using the third-order CWENO scheme, the density of the solution at t=1.95, nXn =480X1920 uniform grids were used, the density variation interval is [0.9, 2.2]. It can be seen from the graph that the CWENO scheme with different weights has good resolution, can capture the vortex structure well, and maintains fairly good symmetry. In particular, there is the largest number of inner vortex and the inner vortex structure of mushroom is clearer by using CWENO-NZ3 then by using CWENO-Z3+.

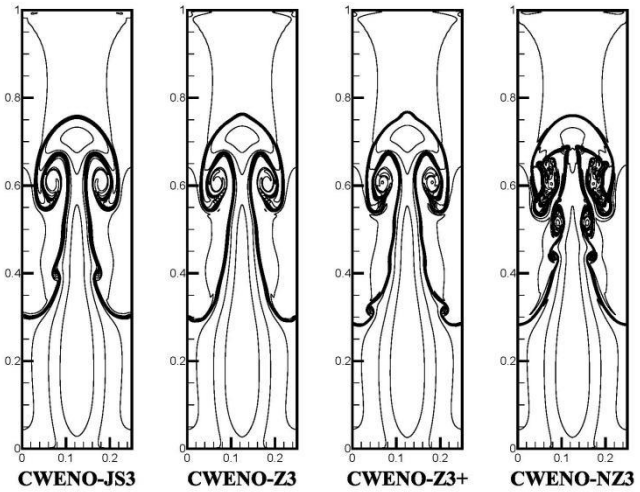

Figs. 3: RT instability problem: 14 density contours at the final time

5. Conclusions

In this paper, based on the finite volume method, we improved the third-order CWENO-Z scheme from two aspects:

Firstly, based on the idea of improving the resolution, we introduced the idea of the WENO-Z+ scheme that enhancing the role of non-smooth factors into the central WENO scheme. By adding the weight of the non-smooth factor, we established the CWENO-Z+ scheme with third-order accuracy.

Secondly, based on the idea of improving the accuracy, combined the ideas of WENO-NP and WENO-JS, by modifying the smoothness factor, we constructed the CWENO-NZ3 scheme.

In this paper, classical examples such as one-dimensional Sod shock tube, Shock-entropy wave interaction, Riemann problem with strong discontinuity and Rayleigh-Taylor instability problem are selected to test CWENO-NZ3 scheme for numerical simulation and compared with the classical third-order WENO scheme. The results show that the two improved central WENO schemes not only improve accuracy and resolution at the extreme points, but also reduce dissipation.

Acknowledgments

Authors wishing to acknowledge from special work by financial support from National Natural Science Foundation of China(11871414).

References

[1] X. D. Liu, S. Osher, T. Chan(1994). Weighted Essentially Non-oscillatory Schemes. Journal of Computational Physics, 115(1): 200-212.
[2] G. S. Jiang, C. W. Shu(1996). Efficient Implementation of Weighted ENO Schemes. Journal of Computational Physics, 126: 202–228.
[3] J. Qiu, C. W. Shu(2003). Hermite WENO schemes and their application as limiters for Runge–Kutta discontinuous Galerkin method: one-dimensional case. Journal of Computational Physics, 193(1): 115–135.
[4] J. Qiu, C. W. Shu(2009). Hermite WENO Schemes and Their Application as Limiters for Runge-Kutta Discontinuous Galerkin Method, III: Unstructured Meshes. Journal of Scientific Computing, 39(2): 293–321.

[5] A. K. Henrick, T. D. Aslam, J. M(2005). Powers. Mapped weighted essentially non-oscillatory schemes: Achieving optimal order near critical points. Journal of Computational Physics. 2005, 207(2): 542-567.
[6] R. Borgers, M. Carmona, B. Costa(2008). An improved weighted essentially non-oscillatory scheme for hyperbolic conservation laws. Journal of Computational Physics, 227(6): 3191-3211.
[7] N. K. Yamaleev, M. H(2009). Carpenter. Third-order energy stable WENO scheme. Journal of Computational Physics, 228(8): 3025-3047.
[8] X. Wu, Y. X. ZHAO(2015). A high-resolution hybrid scheme for hyperbolic conservation laws. InternationalJournal for Numerical Methods in Fluids, 78(3): 162-187.
[9] X. Wu, J. Liang, Y. ZHAO(2016). A new smoothness indicator for third-order WENO scheme. International Journal for Numerical Methods in Fluids, 81(7): 451-459.
[10] W. Xu, W. Wu(2018). Improvement of third-order WENO-Z scheme at critical points. Computers and Mathematics with Applications, 75: 3431–3452.
[11] F. Acker, R. B. de R. Borges, B. Costa(2016). An improved WENO-Z scheme. Journal of Computational Physics, 313: 726-753.
[12] D. Levy, G. Puppo, G. Russo(1999). Central WENO schemes for hyperbolic systems of conservation laws. ESAIM: Mathematical Modelling and Numerical Analysis, 33(3): 547-571.
[13] J. X. Qiu, C. W. Shu(2002). Finite Difference WENO Schemes with Lax--Wendroff-Type Time Discretizations. SIAM Journal on Scientific Computing, 24(6): 2185–2198.
[14] I. Cravero, M. Semplice, G. Visconti(2018). Optimal definition of the nonlinear weights in multidimensional Central WENOZ reconstructions. arXiv.org.
[15] A. K. Henrick, T. D. Aslam, J. M. Powers(2005). Mapped weighted essentially non-oscillatory schemes: achieving optimal order near critical points. Journal of Computational Physics, 207(2): 542-567.
[16] P. D. Lax, X. D. Liu(1998). Solution of Two-Dimensional Riemann Problems of Gas Dynamics by Positive Schemes. SIAM Journal on Scientific Computing, 19(2): 319–340